Evidence for the Eu 4f Character of Conduction-Band Edge at the Eu_2O_3 Surface Studied by Scanning Tunneling Spectroscopy

J.-P. Lehtiö[1], T. Hadamek[2], M. Kuzmin[1,3,*], P. Laukkanen[1], and A. A. Demkov[2]

[1] *Department of Physics and Astronomy, University of Turku, FI-20014 Turku, Finland.*

[2] *Department of Physics, The University of Texas at Austin, Austin, TX 78712, USA.*

[3] *Ioffe Physical-Technical Institute, Russian Academy of Sciences, St. Petersburg 194021, Russian Federation.*

Abstract

Effects of localized Eu 4f levels on the band gap properties of Eu_2O_3 have attracted significant fundamental and technological interest, and the band structure of such thin films has been thoroughly studied by photoelectron spectroscopies (T. Hadamek *et al.*, J. Appl. Phys. 127 (2020) 074101). Here we apply a scanning tunneling spectroscopy (STS) to clarify the character of the conduction band (CB) bottom at the surface of epitaxial Eu_2O_3 grown on GaN(0001)/Si(111) substrates. It is shown that the CB edge is formed solely by an unoccupied Eu 4f state 0.8 eV above the Fermi level at the Eu_2O_3 surface and does not overlap with unoccupied Eu 5d6s states laying more than 2 eV higher than the bottom of the 4f band.

Keywords: thin film; europium sesquioxide; electronic structure; band gap; unoccupied states; scanning tunneling spectroscopy.

1. Introduction

For europium oxide three major forms exist: EuO, Eu_3O_4, and Eu_2O_3. The Eu atoms in the sesquioxide (Eu_2O_3) have the highest possible oxidation state (+3), and therefore, during synthesis the stoichiometry of this form can be precisely achieved under oxygen-rich conditions [1]. Having a dielectric constant of about 14 [2] and a measured band gap of ~4.3-4.4 eV [3,4], Eu_2O_3 is considered to be attractive as a high-K gate dielectric [5]. Also, epitaxial monoclinic B-type Eu_2O_3 can act as a precursor in a topotactic transformation reaction for growing epitaxial rock salt EuO [6], which is an appealing ferromagnetic semiconductor for spintronics [7,8].

Despite its potential technological importance, a number of issues related to the preparation and fundamental properties of Eu_2O_3 still remain unresolved. From the experimental viewpoint, unveiling the fundamental properties, such as the electronic structure, is challenging because of the difficulty to manufacture sufficiently large single crystals of Eu_2O_3 that are required for the reliable characterization of samples. On the other hand, from the theoretical viewpoint, the analysis of electronic structure of Eu_2O_3 is complicated because of the localized semi-core nature of 4f electrons in Eu. In general, the

electronic structure of lanthanide (Ln) sesquioxides can be reasonably determined by taking into account trends occurring across the Ln series, in particular the behavior of the 4f bands [9,10]. Systematic band gap variations across the Ln_2O_3 series can be predicted reasonably well within the assumption that the energy difference of the Ln 5d6s states that dominantly form the conduction band (CB) and the O 2p states that do the valence band (VB) is independent on the atomic number of Ln [10]. For Eu_2O_3 and Yb_2O_3 that exhibit unexpectedly small gaps, there is yet no consensus on the physical reason of such bandgap reduction. This has been assigned to a smaller energy difference of empty Eu (or Yb) 5d6s and occupied O 2p compared to the other Ln sesquioxides, which is not yet confirmed reliably [3]. Moreover, the Eu_2O_3 band gap is still an open issue, because the quantities obtained by different techniques can vary from each other by 2.2-3.8 times, for instance, 1.2–1.84 eV in transport experiments [11–13] and 4.0-4.6 eV in optical measurements [3]. In addition, theoretical methods are unable to solve the above controversy. Density functional theory (DFT) calculations can easily fail in examining the properties of the 4f level, and for this reason, perturbative corrections are needed to describe the ground state more accurately [14]. Using the local spin density approximation with the Hubbard U correction (LSDA + U), an unoccupied (majority spin) Eu 4f "in-gap" state close to the O 2p-derived VB maximum (VBM) that moves to approximately mid-gap for a physically reasonable range of U values (5–7 eV) is found, leading to an energy gap substantially narrower than the Eu 5d6s–O 2p one [14,15]. Using GW and screened-exchange (sX) correlation methods, the empty "in-gap" Eu 4f state moves toward the Eu 5d6s-derived CB, resulting in a gap much closer to the Eu 5d6s–O 2p energy difference [14,16].

In a recent study combining normal and inverse photoemission, the details of the band structure, namely the band gap, ionization energy, and electron affinity, of stoichiometric Eu_2O_3 thin films grown on n-type GaN(0001) have been elucidated [4]. In particular, it has been determined that the directly measured bandgap of Eu_2O_3 is 4.3 eV, which agrees well with the values reported on the basis of optical measurements [7]. The CB bottom is found at 1.0 eV above the Fermi level (EF), leading to a narrower bandgap of Eu_2O_3 as compared to those of the Ln2O3 series. It is assumed in Ref. [4] that this narrowing is caused by weak unoccupied 4f states, strongly hybridized with 5d6s states, near the Eu_2O_3 CB edge, while the bottom of CB in the Ln_2O_3 series is typically determined solely by unoccupied Ln 5d6s states. However, a more detailed band structure near the CB edge of Eu_2O_3 has not been determined experimentally in the earlier studies because it is challenging to probe the empty levels in general. In this work, we utilize a complementary technique,

scanning tunneling microscopy (STS), to shed more light on the nature of the CB edge in Eu_2O_3. Because STS is a surface sensitive method, the presented results clarify in particular the surface properties of Eu_2O_3. We provide evidence that the bottom of CB in Eu_2O_3 has predominantly 4f character and does not overlap with the 5d6s states that lay more than 2 eV higher in energy.

2. Experiments

The experiments were performed in two separate ultra-high vacuum (UHV) systems. The Eu_2O_3 film was grown on GaN(0001)/p-Si(111) substrates at 800 ^oC by MBE; the growth, sample and UHV system details are described in [1,4].The Eu_2O_3 film revealed a streaky reflection high-energy electron diffraction (RHEED) pattern after formation, as shown in Figure 1. The rotational symmetry of the pattern was 6-fold, the same as the underlying GaN susbstrate pattern. When calibrated by the well-known substrate d-spacings, the horizontal streak spacings of the film give a pseudo-hexagonal lattice constant of a_{Eu2O3} = (3.66 ± 0.18) Å for the Eu_2O_3 surface. The thickness of the Eu_2O_3 film was 5.5 nm, determined using the Debye-Scherrer equation on the film peak located at $2\theta = 29.94^o$ in X-ray diffraction with Cu-Kα and the 2θ spacing of the apparent finite-size oscillation from 0^{th} to 1^{st} order peak (see Figure 2). The sample was transferred in air and loaded into another UHV system with the base pressure $<10^{-10}$ mbar, which featured room-temperature Omicron scanning probe microscope, low-energy electron diffraction (LEED), and x-ray photoelectron spectroscopy (XPS). The photoelectron spectra were recorded with the nonmonochromatic Mg Kα (1253.6 eV) x-ray source. The pass energy was 30 eV. The binding energy was calibrated by using a clean Si(111) sample, assuming the binding energy of the Si 2p feature to be 99.4 eV. No charging effects were observed during the acquisition of spectra. Before STS measurements, the sample was heated in O_2 at a pressure in the 10^{-6} mbar range at around 600 ^oC for 30 min. This is required to restore the stoichiometry of the Eu_2O_3 surface, which is shown to reduce significantly upon exposure to air [4]. The sample heating was performed by passing a direct current through the substrate.

The STS measurements were performed along with scanning tunneling microscopy (STM) observations. Several tungsten tips prepared in different ways were used to verify the reproducibility of results and exclude the influence of the tip on the main conclusions. The topography images (400 × 400 points) were taken in the constant-current mode. The plane (linear) background correction was used, and the STM scanner was calibrated by using the well-known vicinal Si(111)(7×7) surface with an array of single and

triple atomic steps. The current-voltage (I-V) spectra were acquired over the well-defined area of the Eu sesquioxide film at every fourth point along every fourth scanning line of the topography image. At these points the STM tip was stopped, the feedback loop disabled (at the chosen tunneling current), and the bias voltage was swept out for measuring an I-V curve shortly. Because of a short period of the I-V measurement, the tip drift was neglected. Finally, the feedback was reactivated for further measurements. As a result, a set of I-V spectra, i.e., $100 \times 100 = 10^4$ curves were acquired for a single topography image. The I-V curves were averaged before further processing. This procedure allowed us to remove random fluctuations. The individual curves can slightly vary from one to another because of instrumental aspects as well as local surface inhomogeneity; however, such variation does not affect the main conclusions. The I-V spectra were numerically differentiated and plotted in the form of normalized differential conductivity - bias voltage curves that are known to reflect the local density of states (LDOS) of probed sample [17,18]. For non-conducting materials the tunneling current as well as the differential conductivity, dI/dV, are zero within the band gap (or tunneling gap), and direct calculations of (dI/dV)/(I/V) from measured spectra are problematic. For this reason, we utilized the elegant approach proposed in Ref. [19], where LDOS is calculated in the form of (dI/dV)/(a+I/V). Here the small constant a is chosen to be 0.01 nA/V. This value is large enough so as not to accentuate the noise signal in the tunneling gap, on one hand, but not as large as to affect the spectral line shape and conclusions, on the other hand.

3. Results and discussion

Figure 3 illustrates the difference in the XPS spectra of the air-exposed sample restored after the transfer by using two different procedures. In Figures 3a and 3b, survey XPS spectra for Eu_2O_3 samples heated at 300 ^oC in UHV and 600 ^oC in oxygen background (at the 10^{-6} mbar pressure) are presented. The range on the binding-energy axis is chosen to present all most important spectroscopic features for the samples. It is seen that the former treatment is not enough to remove carbon contamination from the air exposure, i.e., a strong C 1s peak is present at the binding energy around 285 eV in Figure 3a. In contrast, this peak is lacking after the latter treatment (Fig. 3b), and therefore, the heating at 600 ^oC in O_2 background allows one to restore the film free of carbon contamination, supporting well the results in Ref. [4]. In addition, the VB spectra shown in Figure 3c demonstrate a difference in valence state of Eu atoms for the two samples. This can be reliably determined on the basis of energy splitting of the $4f^6$ and $4f^5$ final-state features that are due to the divalent (Eu^{2+}) and trivalent (Eu^{3+}) configurations, respectively [20,21]. The sample treated by the former

method shows the presence of a notable divalent Eu 4f feature at around 2 eV, in addition to the main Eu^{3+} peak at 7-8 eV, whereas the sample treated by the latter process reveals solely the trivalent Eu species. Thus, the controlled re-oxidation at 600 ^{o}C is an important step to restore the stoichiometric Eu_2O_3 film after the transfer in air, in full agreement with the earlier finding [4]. Note that the O 1s emission (not shown here) also closely resembles that of Ref. [4] after the oxygen treatment.

The long-range order and epitaxial crystalline structure of Eu_2O_3 thin films annealed at 600 ^{o}C in O_2 background has been confirmed by LEED. Figure 4a shows the pseudo-hexagonal (1×1) LEED pattern observed for such films. The pseudo-hexagonal lattice parameter of Eu_2O_3 (a_{Eu2O3} = 3.66 Å) determined on the basis of the post-growth RHEED results (Section 2) corresponds to the lattice mismatch of 14.7% at the Eu_2O_3/GaN(0001) interface (a_{GaN} = 3.19 Å [22]). This lattice mismatch is slightly less than that of GaN(0001)/Si(111) (-16.9%, a_{Si} = 3.84 Å), allowing for epitaxial growth of Eu_2O_3 films on GaN(0001)/Si(111).

The large degree of smoothness and homogeneity of such films is also confirmed by STM. Figure 4b presents a large-scale STM image of Eu_2O_3 (the area is 556 × 314 nm). As the Eu sesquioxide has a relatively wide band gap (4.3 eV) [4], imaging the surface of this oxide by STM is rather challenging and requires specific tunneling parameters. The sample bias voltage used to acquire the STM data in Fig. 4b was – 6.0 V, which lowered the overall resolution and did not allow us to achieve the atomic resolution. Nonetheless, the STM results in Fig. 4b are useful to characterize the surface morphology of the Eu_2O_3 film. A histogram shown in Figure 4c illustrates a roughness analysis of this film on the basis of the above image. Each experimental datapoint (solid circles in Fig. 4c) represents the number of events, i.e., pixels in Fig. 4b at which the tip height (s) is found within the given interval, $s \pm \Delta s$. The total number of intervals for the full range of height variation is chosen to be 100, which defines the interval width of $2\Delta s = 1.935\times10^{-2}$ nm. The height distribution obtained in such a manner is reasonably fitted with a single Gaussian peak which is shown by solid curve. This implies that the grown Eu_2O_3 film is highly homogeneous. Moreover, the Gaussian distribution has the full width at half maximum (FWHM) of 0.67 nm, which indicates that the film is very uniform in thickness (the roughness about 12% of the film thickness). All this suggests that the grown Eu_2O_3 film is uniform, consistent with the STS observations that the DOS curves did not vary significantly over the sample.

STS measurements are not straightforward for Eu_2O_3/GaN/p-Si(111) samples as compared to the semiconductor crystals, such as a vicinal p-Si(111) sample utilized as a

reference in this study, since the Eu_2O_3 films are insulating and rather thick for this extremely surface-sensitive technique. We found that it was helpful to decrease the feedback voltage and/or increase the feedback current for the I-V curve acquisition. This brings the tip into closer approach with the surface.

Figure 5a presents a normalized differential conductivity spectrum taken from the reference sample that was cleaned by rapid flashing at around 1200 ^{o}C. As mentioned in Section 2, this curve reflects the LDOS of the surface. For such measurements, the same STS parameters were also used for the Eu_2O_3 samples discussed below. The bulk band gap of Si is known to be 1.12 eV at room temperature, and Fermi level pinning occurs at 0.7 eV above the VBM for both n-type and p-type Si(111) surfaces [23]. The spectral line shape in Figure 5a agrees with respective data available in literature (e.g., [24]).

STS curves were acquired for the Eu_2O_3/GaN/p-Si(111) samples annealed in O_2 at 600 ^{o}C using experimental parameters similar to those of pristine Si(111). In Figure 5b, we present a family of normalized differential conductivity spectra recorded for the Eu_2O_3 at various feedback current setpoints, I_t = 0.05, 0.10, and 0.15 nA. The decrease of the current setpoint means that the tip height *s*, i.e., the distance from the tip to the surface probed in STS increases. The direction of increasing this distance is marked by the arrow in Figure 5b. Such variation is very important, since it allows one to distinguish the individual electronic states at the Eu_2O_3 surface. In fact, the vacuum decay rates of the wave functions that are associated with inequivalent surface orbitals (or surface states), can be significantly different. Therefore, the predominant contribution to the tunneling current is due to different orbitals when varying the vacuum gap *s*. The more delocalized the probed orbital, the more slowly its contribution to the tunneling current should decrease with increasing tip height, and vice versa. As the 5d6s states are expected to be more delocalized than the semi-core 4f states in the Eu sesquioxide, we presume that the contribution of the former to the tunneling current decreases with *s* slowly and that of the latter much more rapidly. Hence, the Eu 4f states can be readily probed by STS at relatively small tip-sample distances and do not provide notable contribution to the tunneling current at relatively large tip-sample distances, whereas the Eu 5d6s states can notably contribute to the measured signal at both small and large tip-sample distances.

It is known that the tunneling current can be expressed as $I_t \propto \int_0^{eV} \rho_{sub}\,(E)T(E,eV)dE$, where $T(E,eV) = e^{-2\kappa s}$ is the electron transmission

probability, $\kappa = \sqrt{\frac{2m}{\hbar^2}\left[\frac{\left(\phi_{tip}+\phi_{sub}\right)}{2} - E + \frac{eV}{2}\right] + k_{\parallel}^2}$ is the inverse decay length, E is the energy of the probed state, ϕ_{tip} and ϕ_{sub} are tip and sample work functions, respectively, $\rho_{sub}(E)$ is the LDOS of the sample, and $k_{\parallel}$ is the surface-parallel component of the electron momentum [17,18]. Assuming the tunneling current ratio I_{t1}/I_{t2} to be roughly proportional to $\int_0^{eV} e^{-2\kappa s_1} dE \,/\, \int_0^{eV} e^{-2\kappa s_2} dE$ and taking into account typical experimental values and parameters (ϕ_{tip} = 4.5 eV, ϕ_{sub} = 3.2 eV, V = 1.6 and 4.0 V), we can find that the ratio I_{t1}/I_{t2} = 3 (0.15 nA / 0.05 nA) corresponds to s_1/s_2 ~ 1 : (1.6-1.7). That is, a change of tunneling current by a factor of three (from 0.15 to 0.05 nA) requires an increase of the vacuum gap s by 1.6-1.7 times, i.e., the tip should be retracted from the surface by ~60-70%. Definitely, such a shift can cause a drastic change in tunneling electrons to/from localized Eu 4f states, while the effect is expected to be significantly less pronounced for delocalized Eu 5d6s states.

Comparison of spectra in Figure 5b clearly shows that both the spectral lineshape and observed LDOS of Eu_2O_3 are indeed strongly affected by tip height. Below the Fermi level (i.e., 0-V position on the voltage axis), two important features, a strong peak at -1.4 eV and a weak shoulder at -0.3 eV, can be identified. Both of them lay within the bulk Eu_2O_3-film band gap determined by photoemission in Ref. [4]. One possible explanation could be band bending effects leading to variation of the Fermi level position in the present STS experiment. However, the binding energy of the former feature (at 1.4 eV below the Fermi level) is not affected by the variation of experimental parameters, e.g., the s value in Figure 5b. Therefore, we assume that these features are not due to the tip-induced band bending effects.

The other possible explanations of the aforementioned features in Fig. 5b are surface states caused by structural defects or/and intrinsic surface states on the top of the Eu_2O_3 film. In the case of structural defects, the respective features in STS should be observed only locally on the surface, depending on the lateral position of the tip. As already remarked, this was not the case in our experiment, and the features seen at 0.3 and 1.4 eV below the Fermi level in Fig. 5b are well reproduced at different tip locations. Therefore, we rule out the structural defects as the origin of these features.

As for the intrinsic surface states, no additional structure, except for the (1×1) one, has been found on the surface of Eu sesquioxide film, however, Eu and/or O atoms on the film surface have the environments different from the bulk. In principle, this can lead to the appearance of occupied surface states above the VBM of Eu_2O_3. For instance, such states

were observed for Eu^{2+} [4]. Moreover, the presence of both STS features is observed for several Eu_2O_3 samples, and consequently, they are not due to surface contaminations. Comparing the STS results in this study and photoemission data in Ref. [4], one has raised the question why such surface states were not detected in photoelectron spectra. The probing depth of ultraviolet photoelectron spectroscopy (UPS) used in Ref. [4] was 9 Å, and therefore, the techniques can be sufficiently sensitive to the topmost atomic layer. It was also shown in Ref. [4] that probing different atomic subshells in Eu_2O_3 by UPS is not the same at all, based on drastically different photoionization cross-section data for O 2p, Eu 4f, and Eu 6s. In particular, the most prominent contribution to UPS spectra is provided by O 2p states, while those of Eu 4f and Eu 6s are significantly less. Based on such argumentation, we assume that the features at 0.3 and 1.4 eV below the Fermi level in Fig. 5b are not related to O 2p states. Tentatively, these features can be attributed to Eu 4f and Eu 5d6s related surface states. It is important that the feature at -1.4 eV can be observed at all feedback currents and tip heights in Fig. 5b. Therefore, it is unlikely that this state has significant Eu 4f character. Rather, it likely arises from the more delocalized Eu 5d6s states. In contrast, the state at -0.3 eV can be identified only at the closest distance of the tip from the surface (i.e., at the lowest *s*) and is not detected at higher tip heights and *s* values. Hence, we can associate this feature with the occupied 4f orbitals of the surface Eu atoms. Further studies are needed to clarify the origins of these states in more detail.

The spectra above the Fermi level are drastically different from those below E_F. As clearly seen, the curves above E_F are strongly affected by the tip height. The offsets provided on the horizontal axis by linear segments in Figure 5b correspond to the bottom of the CB. Its position is drastically influenced by the *s* value. At the smallest tip-sample distance the CB bottom is found at 0.77 eV above E_F. At the largest tip-sample distance it is located between 3.12 and 3.36 eV. Finally, at intermediate *s* the CB edge lies at 1.76 eV. Thus, the details of the band structure appear to be systematically dependent on the STS feedback current, i.e., the tip height. At first glance, the above variation of the CB edge could be caused, for example, by charging effects. However, the energy position of the feature at 1.4 eV below E_F is not affected by the feedback current, and therefore, we rule out the charging effects. We interpret the variation of the CB edge in Figure 5b in terms of selective probing of different unoccupied states with changing the tip height. When the tip is sufficiently close to the surface (i.e., at the smallest *s*), we assume that the tunneling can efficiently occur into more localized empty Eu 4f states. Hence, the edge of CB measured at the smallest *s* (0.8 eV above the Fermi level) comprises unoccupied Eu 4f state(s). The wave

functions associated with Eu 4f states decay rapidly into vacuum with increasing tip height, and at higher *s*, the dominant contribution to the tunneling current is provided by more delocalized Eu 5d6s states. For this reason, the LDOS bottom determined at the largest *s* (3.12-3.36 eV above E_F) can be understood in terms of electron tunneling into unoccupied 5d6s states of the Eu_2O_3. Interestingly, the slope of linear segments in Figure 5b is systematically dependent on *s*. As seen from this figure, the edge of the LDOS associated with the Eu 4f state (near 0.8 eV) is relatively narrow, while that of the Eu 5d6s state is relatively broad. This is in good agreement with the earlier LDOS calculations (see e.g. Fig. 3 in [4]).

Thus, the present STS results indicate that the CB bottom on the Eu_2O_3 surface is caused by unoccupied Eu 4f states and located ~0.8 eV above the Fermi level. This value is consistent with the CB edge of Eu_2O_3 films determined by inverse photoemission (1.0 eV [4]). Based on STS, the bottom of the unoccupied Eu 5d6s band is found at 3.1-3.4 eV above the Fermi energy. Therefore, the unoccupied Eu 5d6s states do not overlap with the CB edge of Eu_2O_3, and the latter solely has Eu 4f character. Thus, the results show that the reduced band gap of Eu_2O_3 is not due to the decreased binding energy of unoccupied Eu 5d6s states, but is determined by the energy gap between the occupied O 2p states and the portion of unoccupied Eu 4f states, which fully forms the bottom of CB in the Eu sesquioxide.

4. Summary

The electronic structure of the Eu_2O_3 surface was investigated by STS using thin (5.5 nm) epitaxial Eu_2O_3 films on a GaN/p-Si(111) template. In good agreement with the previous finding [4], we found that the well-defined stoichiometric Eu_2O_3 film required annealing at 600 ^oC in O_2 background (10^{-6} mbar) after exposure to air. STS measurements with varying tip-sample distances show that the bottom of the CB is formed by unoccupied Eu 4f states 0.8 eV above E_F and does not overlap with the bottom of unoccupied Eu 5d6s band. The latter is found 3.1-3.4 eV above E_F. The CB minimum of Eu_2O_3 has Eu 4f character, and the bulk gap of Eu sesquioxide is due to the energy difference of empty Eu 4f and filled O 2p states.

The STS data also revealed two occupied surface states energetically lying within the bulk band gap on the Eu_2O_3 surface. The state 0.3 eV below the Fermi energy can be identified only at the smallest tip-sample distances and is assigned to occupied 4f states of surface Eu atoms. The other surface state is found at 1.4 eV below E_F and not affected practically by the tip-sample distance. This state is more delocalized than the former and

tentatively assigned to Eu 5d6s states. More studies are needed for further clarification of their origins.

Acknowledgements

We thank Agham Posadas for helpful discussions and critically reading the manuscript. The work at the University of Texas at Austin is supported by the National Science Foundation under grant DMR-1507970. Three of us (JPL, MK, and PL) also acknowledge the support from the Academy of Finland (via the project #296469).

References

* Corresponding author. E-mail: m.kuzmin@mail.ioffe.ru, mikuzm@utu.fi.

[1] T. Hadamek, D. Shin, A.B. Posadas, A.A. Demkov, S. Kwon, Q. Wang, M. Kim, Hexagonal to monoclinic phase transformation in Eu $_2$ O $_3$ thin films grown on GaN (0001), Appl. Phys. Lett. 111 (2017) 142901. https://doi.org/10.1063/1.4997021.

[2] D. Xue, K. Betzler, H. Hesse, Dielectric constants of binary rare-earth compounds, J. Phys. Condens. Matter. 12 (2000) 3113–3118. https://doi.org/10.1088/0953-8984/12/13/319.

[3] A.V. Prokofiev, A.I. Shelykh, B.T. Melekh, Periodicity in the band gap variation of Ln2X3 (X = O, S, Se) in the lanthanide series, J. Alloys Compd. 242 (1996) 41–44. https://doi.org/10.1016/0925-8388(96)02293-1.

[4] T. Hadamek, S. Rangan, J. Viereck, D. Shin, A.B. Posadas, R.A. Bartynski, A.A. Demkov, Stoichiometry, band alignment, and electronic structure of Eu2O3 thin films studied by direct and inverse photoemission: A reevaluation of the electronic band structure, J. Appl. Phys. (2020). https://doi.org/10.1063/1.5139227.

[5] L.-C. Yen, C.-W. Hu, T.-Y. Chiang, T.-S. Chao, T.-M. Pan, Electrical and reliability characteristics of polycrystalline silicon thin-film transistors with high-κ Eu $_2$ O $_3$ gate dielectrics, Appl. Phys. Lett. 100 (2012) 173509. https://doi.org/10.1063/1.4705472.

[6] T. Mairoser, J.A. Mundy, A. Melville, D. Hodash, P. Cueva, R. Held, A. Glavic, J. Schubert, D.A. Muller, D.G. Schlom, A. Schmehl, High-quality EuO thin films the easy way via topotactic transformation, Nat. Commun. 6 (2015) 7716. https://doi.org/10.1038/ncomms8716.

[7] T.S. Santos, J.S. Moodera, Observation of spin filtering with a ferromagnetic EuO tunnel barrier, Phys. Rev. B. 69 (2004) 241203. https://doi.org/10.1103/PhysRevB.69.241203.

[8] K.J. Kormondy, L. Gao, X. Li, S. Lu, A.B. Posadas, S. Shen, M. Tsoi, M.R. McCartney, D.J. Smith, J. Zhou, L.L. Lev, M.A. Husanu, V.N. Strocov, A.A. Demkov, Large positive linear magnetoresistance in the two-dimensional t2gelectron gas at the EuO/SrTiO3interface, Sci. Rep. 8 (2018) 1–9. https://doi.org/10.1038/s41598-018-26017-z.

[9] E. Rogers, P. Dorenbos, E. van der Kolk, Systematics in the optical and electronic

properties of the binary lanthanide halide, chalcogenide and pnictide compounds: an overview, New J. Phys. 13 (2011) 093038. https://doi.org/10.1088/1367-2630/13/9/093038.

[10] E. van der Kolk, P. Dorenbos, Systematic and Material Independent Variation of Electrical, Optical, and Chemical Properties of Ln Materials over the Ln Series (Ln = La, Ce, Pr, ..., Lu), Chem. Mater. 18 (2006) 3458–3462. https://doi.org/10.1021/cm060775s.

[11] J.B. Goodenough, Electron Transport in Transition-Metal and Rare-earth Oxides, in: M.S. Seltzer, R.I. Jaffee (Eds.), Defects Transp. Oxides, Springer US, Boston, MA, 1974: pp. 55–82. https://doi.org/10.1007/978-1-4615-8723-1_3.

[12] H.B. Lal, K. Gaur, Electrical conduction in non-metallic rare-earth solids, J. Mater. Sci. 23 (1988) 919–923. https://doi.org/10.1007/BF01153989.

[13] G.V.S. Rao, S. Ramdas, P.N. Mehrotra, C.N.R. Rao, Electrical transport in rare-earth oxides, J. Solid State Chem. 2 (1970) 377–384. https://doi.org/10.1016/0022-4596(70)90095-2.

[14] H. Jiang, P. Rinke, M. Scheffler, Electronic properties of lanthanide oxides from the G W perspective, Phys. Rev. B. 86 (2012) 125115. https://doi.org/10.1103/PhysRevB.86.125115.

[15] G. Concas, J.K. Dewhurst, A. Sanna, S. Sharma, S. Massidda, Anisotropic exchange interaction between nonmagnetic europium cations in Eu 2 O 3, Phys. Rev. B. 84 (2011) 014427. https://doi.org/10.1103/PhysRevB.84.014427.

[16] R. Gillen, S.J. Clark, J. Robertson, Nature of the electronic band gap in lanthanide oxides, Phys. Rev. B. 87 (2013) 125116. https://doi.org/10.1103/PhysRevB.87.125116.

[17] J. Tersoff, D.R. Hamann, Theory and Application for the Scanning Tunneling Microscope, Phys. Rev. Lett. 50 (1983) 1998–2001. https://doi.org/10.1103/PhysRevLett.50.1998.

[18] J. Tersoff, D.R. Hamann, Theory of the scanning tunneling microscope, Phys. Rev. B. 31 (1985) 805–813. https://doi.org/10.1103/PhysRevB.31.805.

[19] M. Prietsch, A. Samsavar, R. Ludeke, Structural and electronic properties of the Bi/GaP(110) interface, Phys. Rev. B. 43 (1991) 11850–11856. https://doi.org/10.1103/PhysRevB.43.11850.

[20] F. Gerken, Calculated photoemission spectra of the 4f states in the rare-earth metals, J. Phys. F Met. Phys. 13 (1983) 703–713. https://doi.org/10.1088/0305-4608/13/3/021.

[21] N. Maartensson, B. Reihl, W.-D. Schneider, V. Murgai, L.C. Gupta, R.D. Parks, Highly resolved surface shifts in a mixed-valent system: EuPd2Si2, Phys. Rev. B. 25 (1982) 1446–1448. https://doi.org/10.1103/PhysRevB.25.1446.

[22] S.Q. Zhou, A. Vantomme, B.S. Zhang, H. Yang, M.F. Wu, Comparison of the properties of GaN grown on complex Si-based structures, Appl. Phys. Lett. 86 (2005) 81912. https://doi.org/10.1063/1.1868870.

[23] W. Mönch, Semiconductor surfaces and interfaces, Springer series in surface science,

Vol. 26, Springer Verlag, Berlin, 1993.

[24] J. Schmeidel, H. Pfnür, C. Tegenkamp, Coulomb blockade effects in Ag/Si(111): The role of the wetting layer, Phys. Rev. B. 80 (2009) 115304. https://doi.org/10.1103/PhysRevB.80.115304.

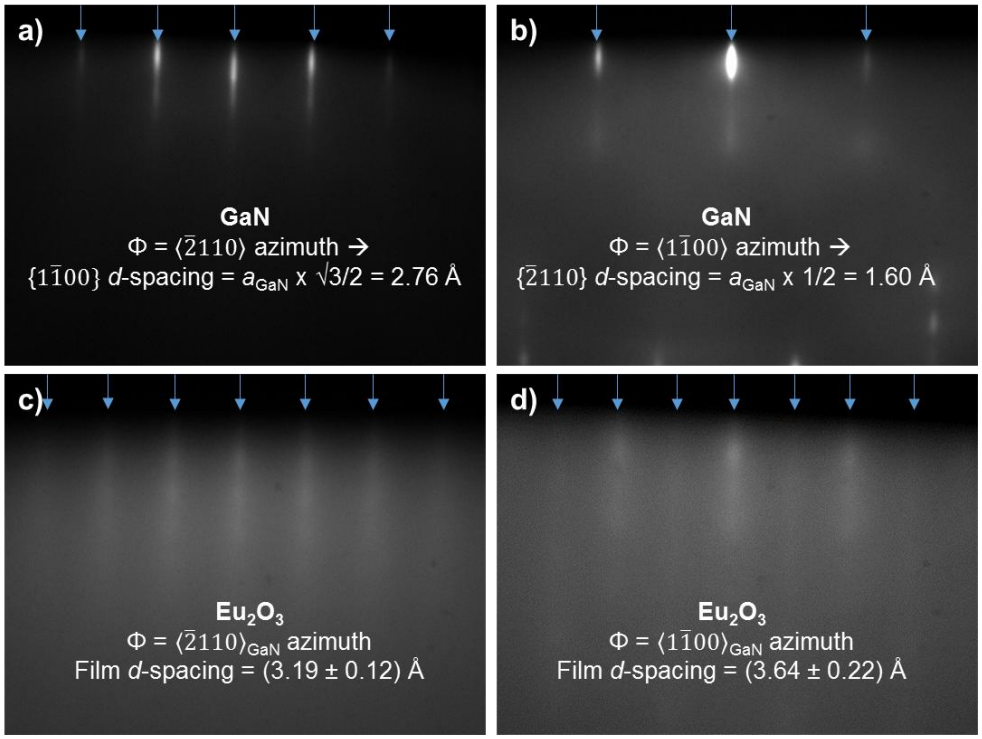

Figure 1: RHEED patterns along the GaN [$\bar{2}$110] azimuth (a) & c)) and along the GaN [1$\bar{1}$10] azimuth (b) & c)), before and after Eu_2O_3 growth. The streak pattern of the Eu_2O_3 film shows a 6-fold rotational symmetry like the underlying GaN substrate. When calibrated by the well-known substrate d-spacings, the horizontal streak spacings (highlighted by blue arrows) give a pseudo-hexagonal lattice constant of a = (3.66 ± 0.18) Å for the film surface. The Eu_2O_3 pattern on the [1$\bar{1}$10] azimuth shows weaker"½ order" streaks that could be related to a surface reconstruction or multi-domain structure.

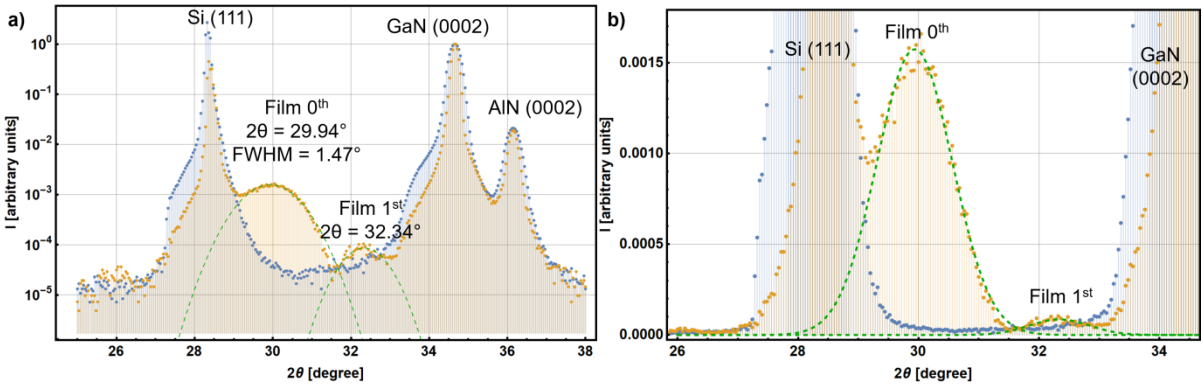

Figure 2: 2θ-ω X-ray diffraction curves using Cu-Kα radiation of a bare GaN/AlN/Si(111) substrate (blue) and a 5.5 nm Eu_2O_3 film on the GaN/AlN/Si(111) substrate (yellow). The difference in the shape of the substrate peaks is caused by the use of slightly different X-ray optics. a) logarithmic intensity scale, b) linear intensity scale.

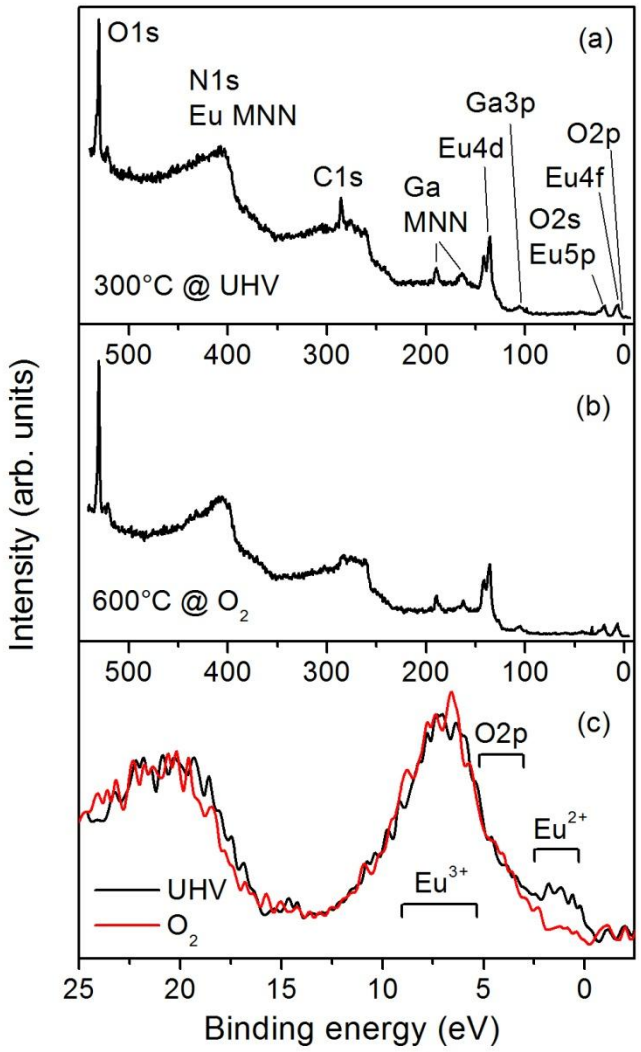

Figure 3. X-ray photoelectron (XPS) survey spectra for Eu_2O_3 film after (a) vacuum heating at 300 ^oC and after (b) heating in O_2 background around 600 ^oC. The assignment of main features is made in (a). (c) Valence band spectra for the both. The binding energy ranges where Eu 4f emission occurs from the divalent and trivalent Eu atoms (Eu^{2+} and Eu^{3+}, respectively) are shown.

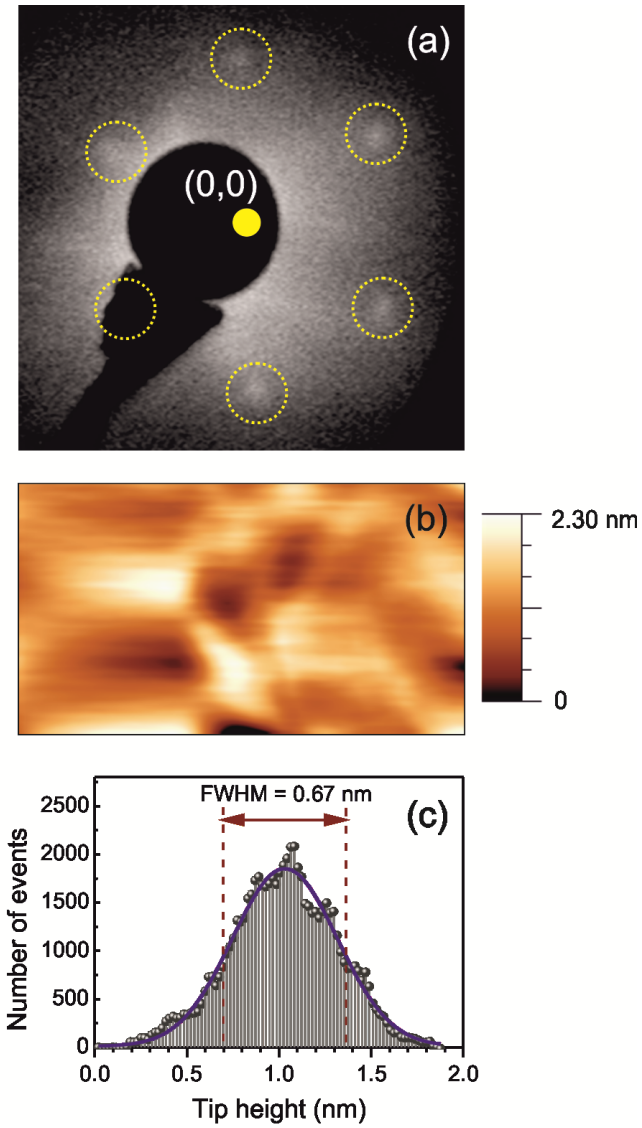

Figure 4. (a) Low-energy electron diffraction (LEED) pattern from the Eu_2O_3 film after heating in O_2 at 600 ^oC. The (1×1) spots are outlined. The position of (0,0) spot is shown by solid cicrle. (b) STM image from Eu_2O_3. The sample bias voltage is -6.0 V and the tunneling current 0.05 nA. The scanning area is 556 × 334 nm. (c) Roughness histogram taken from the STM image in (b). The experimental data are shown by circles. The fitting curve (solid curve) has the Gaussian line shape. The full width at half maximum (FWHM) is 0.67 nm.

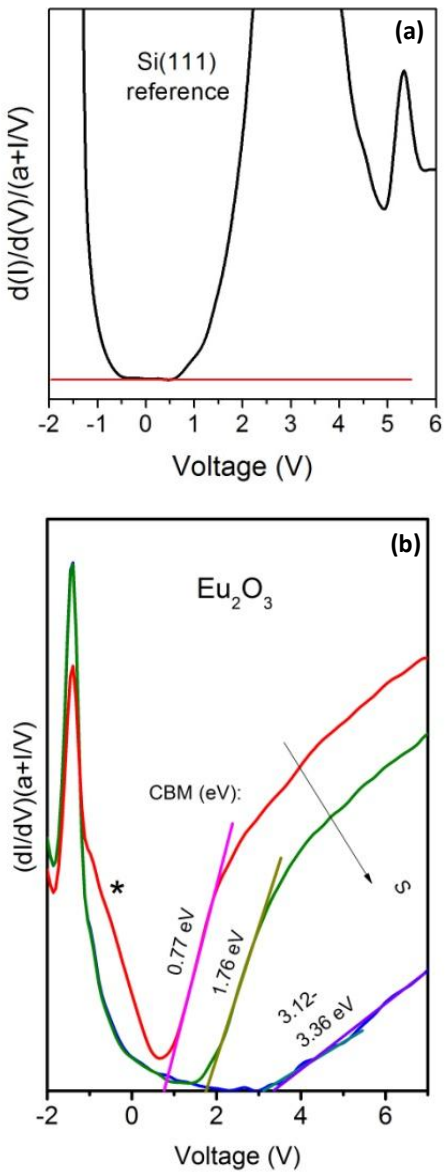

Figure 5. (a) Normalized differential conductivity – bias voltage curve measured by STS for the reference Si(111) sample. The curve reflects the LDOS of the surface. (b) Similar curves measured for the Eu_2O_3 film at various feedback currents (I_t) changing the tunneling gap between the sample and the tip (s). The arrow shows the direction of increasing the value of s. The LDOS observed at the smallest s (red curve) is acquired at I_t = 0.15 nA and LDOS observed at the highest s is acquired at I_t = 0.05 nA (blue curve). The asterix points out the state at 0.3 eV below the Fermi level, detected at 0.15 nA (see the text).